Inner-shell charging of multiwalled carbon nanotubes

M. Zdrojek,[1,2] T. Heim,[3] D. Brunel,[1] A. Mayer,[4] and T. Mélin[1,*]

[1]*Institut d'Electronique de Microélectronique et de Nanotechnologie, CNRS-UMR 8520, Département ISEN, Avenue Poincaré, BP 60069, 59652 Villeneuve d'Ascq Cedex, France*

[2]*Faculty of Physics, Warsaw University of Technology, Koszykowa 75, 00-662 Warsaw, Poland*

[3]*Interdisciplinary Research Institute, CNRS-FR 2963, c/o IEMN, Avenue Poincaré, BP 60069, 59652 Villeneuve d'Ascq Cedex, France*

[4]*Laboratoire de Physique du Solide, Facultés Universitaires Notre-Dame de la Paix, 61 Rue de Bruxelles, B-5000 Namur, Belgium*

(Received 13 November 2007; published 7 January 2008)

The electrostatic properties of individual multiwalled carbon nanotubes (MWCNTs) have been investigated from charge injection and electrostatic force microscopy experiments. The MWCNT linear charge densities analyzed as a function of the nanotube diameters are found to differ from classical capacitive predictions by one order of magnitude and correspond to the response of MWCNTs in the external electric field generated at the microscope tip. The fact that MWCNTs can hold an out-of-equilibrium charge is attributed to the inner-shell charging, as a result of the MWCNT finite transverse polarizability and of the intercalation of semiconducting and metallic shells.

DOI: 10.1103/PhysRevB.77.033404 PACS number(s): 73.63.Fg, 68.37.Ps, 73.22.−f, 73.23.−b

Single and multiwalled carbon nanotubes (CNTs) have been extensively studied in the past decade for their one-dimensional transport properties. However, the electrostatics of CNTs remains a quite open field of experimental and theoretical investigation in spite of the fundamental interest on it for CNT-based electronic devices such as sensors, field effect transistors, and nonvolatile memories,[1,2] for nanoelectromechanical systems,[3,4] and for dielectrophoresis developments.[5] Recent work on single-walled carbon nanotubes (SWCNTs) have drawn a border line between classical-like electrostatic properties, e.g., the spatial charge distribution in SWCNTs (Ref. 6), and quantum properties, such as quantum capacitance effects,[7,8] which highlight the interplay between Coulomb interactions and the SWCNT density of states. However, little experimental work has been performed so far on the electrostatic properties of multiple stacked or rolled graphene layers, in which complex interactions occur due to intershell couplings.[9–11]

In this article, we investigate the electrostatic response of individual multiwalled nanotubes (MWCNTs) upon local charging from an atomic force microscopy tip. The measured nanotube linear charge densities are found to deviate from capacitive predictions by more than one order of magnitude. From an analysis of the charge densities as a function of the nanotube diameters, we demonstrate that MWCNTs respond to applied external electric fields and carry an inner-shell charge as a result of their finite transverse polarizability and of the intercalation of semiconducting and metallic shells.

Charge injection and electrostatic force microscopy experiments have been conducted using an atomic force microscope (multimode, Veeco Instruments) operated under dry nitrogen atmosphere. We used Pt-Ir metal-coated cantilevers with spring constant of 1–3 N/m and typical resonance frequency of 75 kHz. Purified nanotubes grown by chemical vapor deposition were dispersed from dichloromethane solutions on a 200 nm thick silicon dioxide layer thermally grown from a doped silicon wafer. Individual CNTs are localized by tapping-mode topography imaging and charged by local contact with the tip biased at the injection voltage V_{inj} [Fig. 1(a)].[12–14] After injection, the CNT charge state is then measured by electrostatic force microscopy (EFM). In this process, the tip is lifted at a distance $z \simeq 100$ nm above the sample surface to discard short-range surface forces, and the cantilever resonance frequency shifts are recorded as a probe of electrostatic force gradients acting on the tip biased at a detection voltage V_{EFM} [Fig. 1(b)]. In practice, topography and EFM scan lines are interleaved, so that both topography and EFM images are recorded simultaneously.

Experimentally, three distinct behaviors can be observed upon local charging of CNTs, depending on whether the injected charge is (i) stored in the CNT, (ii) emitted by the CNT to surface traps in the SiO_2 layer, or (iii) stored in part in the CNT and in oxide traps. The separation of these effects has been described in detail previously.[14] It is illustrated in Fig. 1 for a MWCNT with 20 nm diameter [see topography image in Fig. 1(c1)], a MWCNT with diameter of 18 nm [Fig. 1(d1)], and a SWCNT with diameter of 3 nm [Fig. 1(e1)]. EFM images acquired prior to charging are shown, respectively, in Figs. 1(c1), 1(d2), and 1(e2). CNTs appear here as dark features (negative frequency shifts) due to their attractive capacitive interaction with the tip. EFM scans acquired after charge injection with the tip biased at $V_{inj} = -6$ V for 2 min are shown in Figs. 1(c3), 1(d3), and 1(e3). The injected electrons correspond here to bright features (positive frequency shifts) as a result of their repulsion with the negatively biased EFM tip. For the 20 and 18 nm diameter CNTs, EFM scans after charging reveal abrupt CNT discharges [arrows in Figs. 1(c3) and 1(d3)]. The occurrence of abrupt discharges demonstrates that MWCNTs can retain out-of-equilibrium charges after injection. It also allows to estimate the fraction of charge which is stored in oxide traps along the nanotubes.[14] Hence, the EFM image of the 20 nm diameter MWCNT after the abrupt discharge [Fig. 1(c3), lower part] is nearly identical to the EFM image prior to injection [Fig. 1(c2)] and thus displays almost no oxide charging, while the EFM image of the 18 nm MWCNT after discharge [Fig. 1(d3), lower part] shows a substantial contribution of oxide charge in the form of a bright halo surround-

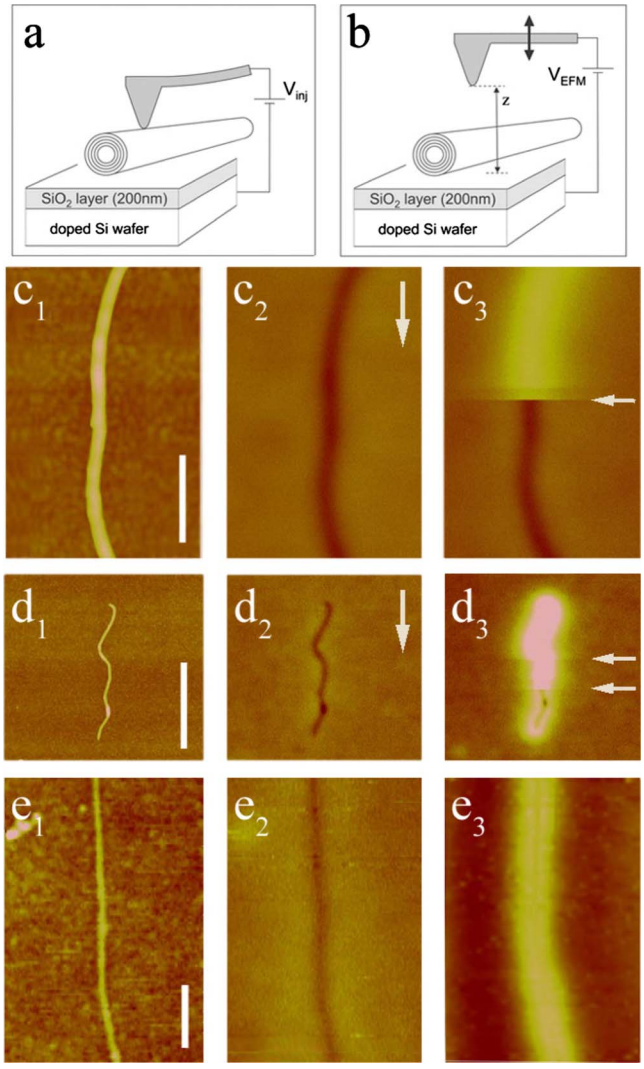

FIG. 1. (Color online) (a) Schematics of the charge injection experiments, in which nanotubes deposited on 200 nm thick SiO_2 layer are addressed with an atomic force microscope tip biased at an injection voltage V_{inj} with respect to the substrate. (b) CNT charge detection in the EFM mode. The electrostatic interaction between the cantilever and the charged CNT is detected from the resonance frequency shift of the cantilever polarized at the detection voltage V_{EFM} and oscillated at a distance z above the sample ($z \simeq 100$ nm). (c1) Topography image (50 nm z scale) of a MWCNT with 20 nm diameter. The scale bar is 300 nm. (c2) EFM image (20 Hz frequency scale) prior to charge injection. The detection voltage is $V_{EFM}=-2$ V. The image was scanned from top to bottom as sketched by the vertical arrow. (c3) EFM image ($V_{EFM}=-2$ V, 20 Hz scale) after a charge injection experiment using $V_{inj}=-6$ V for 2 min. The abrupt CNT discharge occurring during the scan is indicated by the horizontal arrow. (d1) Topography image (50 nm z scale) of an 18 nm diameter MWCNT. The scale bar is 1 μm. (d2) EFM image ($V_{EFM}=-2$ V, 10 Hz scale) prior to injection. (d3) Same image after charge injection using $V_{inj}=-6$ V for 2 min. Two abrupt discharges occur during scanning from top to bottom. (e1) Topography image (12 nm z scale) of a SWCNT of diameter of 3 nm. The scale bar is 300 nm. (e2) EFM image ($V_{EFM}=-3$ V, 20 Hz scale) prior to injection. (e3) Same image after charge injection using $V_{inj}=-6$ V for 2 min.

ing the CNT capacitive footprint. Finally, a careful analysis of EFM data for the SWCNT of Fig. 1(e)[13] has shown that Fig. 1(e3) is dominated by the charge stored in SiO_2 traps.

To understand the electrostatics of MWCNTs in spite of the varied phenomenological behaviors observed upon charging, we performed a quantitative analysis of the CNT linear charge densities. The crucial issue here is to go beyond plane capacitor geometry models,[12] which are by essence restricted to semiquantitative estimations. Truly quantitative charge measurements are obtained as follows. We analyze EFM images [e.g., Figs. 1(c)–1(e)] by comparing the CNT capacitive frequency shift Δf_c measured prior to charging with the additional frequency shift Δf_λ observed after charging the CNT with a linear charge density λ and compute the ratio $\mathcal{R}=\Delta f_\lambda/\Delta f_c$. The advantage of this normalization procedure[15] is that the ratio $\mathcal{R}$ provides an intrinsic measurement of the CNT charge density in a given tip-substrate geometry. In particular, $\mathcal{R}$ does not depend on the spring constant of the cantilever, which enables direct comparisons between charging experiments on different CNTs. To compute the linear charge density λ from the ratio $\mathcal{R}$, we extended the numerical calculations of Ref. 15 by solving the Poisson equation in a three-dimensional geometry, in which the EFM tip is taken as conical (25° half-angle) with a hemispherical apex of radius of 15 nm. The SiO_2 layer is modeled as a dielectric film with relative constant $\varepsilon_{ox}=4$, and nanotubes are described as cylinders of high relative dielectric constant.[16] The relationship between $\mathcal{R}=\Delta f_\lambda/\Delta f_c$ and the linear charge density λ is then obtained without any adjustable parameter from calculating the z component of force gradients at the EFM tip in the absence and in the presence of the neutral and of the charged CNT on the SiO_2 surface.[15]

We represented in Fig. 2 the experimental linear charge densities obtained from EFM data for a set of charge injection experiments performed on 18 MWCNTs (full symbols) and 7 SWCNTs (open symbols), with diameter d_{CNT} in the 1–40 nm range. Experimentally, we used injection voltages V_{inj} between −4 and −10 V and subsequently normalized the charge densities by V_{inj}. For each CNT, we determined whether the charge was detected in the CNT (squares), trapped on the SiO_2 surface (diamonds), or partially in the CNT and in oxide traps (circles). Results of capacitive predictions for metal cylinders are also shown in Fig. 2 (top curves). Curve (a) corresponds to the density expected for a cylinder-plane capacitance in a medium with average dielectric constant $\varepsilon=(1+\varepsilon_{ox})/2$ to account for the geometry of the CNT deposited on the oxide layer of relative dielectric constant $\varepsilon_{ox}=4$. Points shown in (b) have been obtained from three-dimensional Poisson calculations in the geometry depicted in Fig. 1(a). The two capacitive predictions in (a) and (b) only differ by a constant prefactor.

At this stage, two conclusions can be drawn from the comparison between the experimental data points and curves labeled (a) and (b) in Fig. 2:

(i) Experimental linear charge densities exhibit (within experimental accuracy) a similar variation law as a function of d_{CNT} irrespective of the actual location of the charge, i.e., whether the charge is mostly injected in the CNTs, in the oxide surface, or partially in CNTs and in oxide traps.

(ii) Charge densities are found typically one decade below

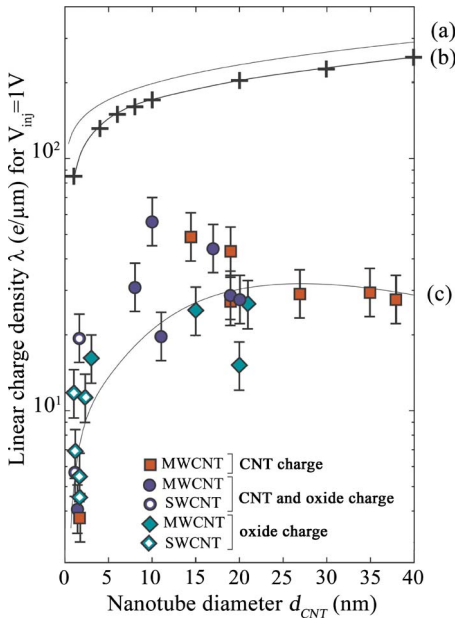

FIG. 2. (Color online) (a) Plot of the CNT linear charge density (in e/μm) normalized by V_{inj} as a function of the CNT diameter d_{CNT}. Experimental data points correspond to charge injection experiments performed in multiwalled and single-walled CNTs with injection voltage $-4\ \mathrm{V} \leqslant V_{inj} \leqslant -10\ \mathrm{V}$. Experimental linear charge densities have been measured from the ratio between charge and capacitive frequency shifts and then normalized by V_{inj}. The top curves correspond to densities expected for metal cylinders. Curve (a) is derived from the cylinder-plane capacitance using a dielectric constant $\varepsilon=(1+\varepsilon_{ox})/2$. Points in (b) are obtained from three-dimensional Poisson calculations with the EFM tip in contact with the CNT as in Fig. 1(a). The line in (b) is a guide to the eye. Finally, curve (c) corresponds to linear charge densities expected from the inner-shell charging of nanotubes as a response to the electric field generated by the EFM tip.

curves (a) and (b). Classical capacitance predictions therefore *do not* correspond to experimental results. They also account neither for the strong variations of experimental charge densities for small d_{CNT} values nor for the saturation and the decrease of densities observed for large d_{CNT} values.

To explain these features, we took into account the response of MWCNTs in the normal electric field E generated at the EFM tip located at a distance d_{CNT} above the oxide layer of thickness d_{ox}. This external field acts as a transverse field with respect to the CNTs deposited on the surface and is screened by the MWCNT multiple shells.[17] Assuming the electronic states of the nanotube shells to be uniformly delocalized along the shell circumference, they will fall at an average potential $E \times d_{CNT}/2$ below that of the EFM tip prior to charging. The equilibrium during the injection is reached when the nanotube carries a net linear charge density λ so as to reach the EFM tip potential. This determines the relationship between the nanotube linear charge density λ and the nanotube diameter d_{CNT}:

$$\lambda = \pi\varepsilon_0/\ln(4d_{ox}/d_{CNT})E \times d_{CNT}. \quad (1)$$

This expression is plotted and labeled (c) in Fig. 2 using values for the transverse field E derived from numerical calculations in the spherical-conical tip geometry. Results fall in good agreement with experimental data, and they reproduce, in particular, the sharp variations of λ for small d_{CNT} values and the saturation and decrease of charge densities observed for large d_{CNT} values. This behavior is dominated by the variations of $E \times d_{CNT}$ as a function of d_{CNT}, while the capacitive prefactor in Eq. (1) only weakly varies with d_{CNT}, as seen from curves (a) and (b). This overall agreement between Eq. (1) and experimental data points demonstrates that MWCNTs get charged as a response to the external applied electric field E and not as a pure capacitive response to the injection bias V_{inj}. Residual discrepancies can nonetheless be observed in Fig. 2. Experimental data points are seen to overestimate the curve labeled (c) especially around $d_{CNT} \simeq 10$ nm and also display a non-negligible dispersion. These discrepancies can be tentatively assigned (i) to the simplified conical-spherical tip geometry used in the numerical calculation of E as a function of d_{CNT}, as compared with actual EFM tip geometries, (ii) to the experimental dispersion in EFM tip apex radii (and thus of E), on which the linear charge is directly dependent, as seen from Eq. (1), and (iii) to the possible accumulation of charge around the CNTs when trapped in the SiO_2 layer. The detailed investigation of these mechanisms, however, falls beyond the scope of this paper.

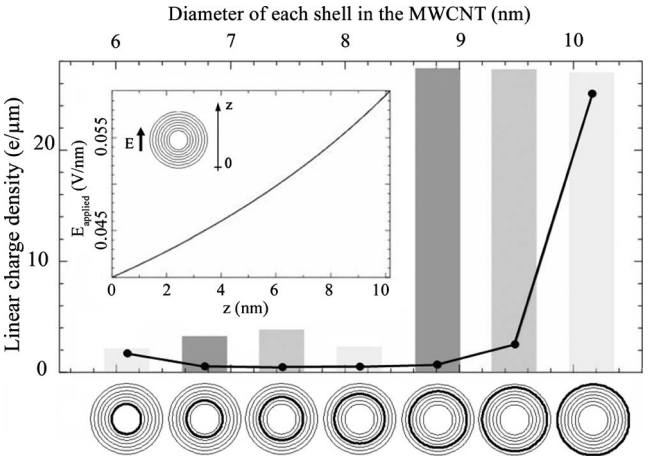

FIG. 3. Plot of the linear charge density associated with each shell of a MWCNT that is characterized by an inner and an outer diameter of 6.1 and 10.2 nm, respectively. The MWCNT is subjected to the same external electric field as in experimental conditions (see inset). The charges are provided by a reservoir representative of the tip that is situated just above the MWCNT at $z=10.2$ nm. These results are obtained by applying the charge-dipole model of Ref. 18. The solid line indicates the results obtained when all shells are metallic. The other results (histograms) are obtained for MWCNTS for which only one shell out of three is metallic (no charge is carried by semiconducting shells). Three MWCNTS have been considered, with the outermost metallic shell, respectively, at the surface of the MWCNT (light gray) and one layer (medium gray) and two layers (dark gray) below the surface.

To get a further insight into the actual location of the injected charges in the CNT shells, we computed the response of a MWCNT in a transverse electric field in the framework of the charge-dipole formalism of Ref. 18. This model is based on the representation of the carbon atoms by

net electric charges and dipoles, which are determined from the minimization of the electrochemical energy of the system. In this context, it is the self-energy of the atomic charges that limits their ability to accumulate on a single shell (the self-energy accounts for the repulsion between charges situated on the same atomic site). To simulate the experimental conditions of this paper, we considered a MWCNT with internal and external diameters of 6.1 and 10.2 nm, respectively (seven shells in total), placed in an external field of average value of 0.05 V/nm (see Fig. 3, inset). By assuming in the first step that all shells are metallic, we find a total linear charge density of 30 e/μm, in fair agreement with experimental values. In this metallic model, however, the charge is mostly stored in the MWCNT outer shell (see Fig. 3, solid line), while all subsurface shells only carry low charge densities.

We considered in the second step the more realistic situation where only one MWCNT shell out of three is metallic (and thus able to accommodate additional charges) while the other two are semiconducting. We calculated (Fig. 3, histograms) the charge densities for three distinct MWCNTs in which the outermost metallic shell is, respectively, at the surface of the MWCNT (light gray) and one layer (medium gray) and two layers (dark gray) below the surface. At equilibrium, the charge is found to be essentially injected in the outermost metallic shell of the MWCNT, and therefore located one or two layers below the nanotube surface (see Fig. 3). The calculated inner-shell linear charge of average density of 27 e/μm falls close to the experimental linear charge densities of Fig. 2. These results agree with the experimental data of Figs. 1(c) and 1(d), in which the abrupt discharge events demonstrate experimentally that a net charge can be stored in MWCNT shells. Results are also consistent with the observation of charges stored in SiO_2 traps below the nanotubes, since this trapping behavior can be expected when the outermost layer of the MWCNT is of metallic character. We believe these observations are altogether specific of multiwalled carbon nanotubes, in which metallic shells can be intercalated between semiconducting shells acting as barriers. The charge retention in MWCNTs as observed in Figs. 1(c) and 1(d) is not expected for purely metallic systems, for which charge would be trapped in the oxide. Finally, numerical calculations show that the metallic shell that follows the outermost metallic shell (when moving inward the MWCNT) can also carry a charge with an $\simeq 3$ e/μm average density. The insertion of semiconducting shells between the metallic ones thus increases the depth reached by the injected charge.

This work constitutes a demonstration of inner-shell charging of MWCNTs. This behavior may be used in memory or sensor devices. The actual control of intershell couplings from the structural properties of MWCNTs appears as a fundamental issue to build such devices.

We are indebted to H. Diesinger, D. Stiévenard, D. Deresmes, C. Delerue, L. Wirtz, W. Gebicki, and L. Adamowicz for fruitful discussions and technical help. This work was done in the framework of the CNRS GDR-E No. 2756, and supported in part by the ANR Grant No. JC05_46152. M.Z. acknowledges support by Polish Ministry of Research under Grant No. N202 050 31/2777.

*thierry.melin@isen.iemn.univ-lille1.fr

[1] See, e.g., A. Javey, J. Guo, Q. Wang, M. Lundstrom, and H. Dai, Nature (London) **424**, 654 (2003).
[2] M. S. Fuhrer, B. M. Kim, T. Dürkop, and T. Brintlinger, Nano Lett. **2**, 755 (2002).
[3] See, e.g., A. M. Fennimore, T. D. Yuzvlnsky, W. Q. Han, M. S. Fuhrer, J. Cummings, and A. Zettl, Nature (London) **424**, 408 (2003).
[4] D. Garcia-Sanchez, A. San Paulo, M. J. Esplandiu, F. Perez-Murano, L. Forró, A. Aguasca, and A. Bachtold, Phys. Rev. Lett. **99**, 085501 (2007).
[5] See, e.g., R. Krupke, F. Hennrich, M. M. Kappes, and H. v. Löhneysen, Nano Lett. **4**, 1395 (2004).
[6] P. Keblinski, S. K. Nayak, P. Zapol, and P. M. Ajayan, Phys. Rev. Lett. **89**, 255503 (2002).
[7] S. Ilani, L. A. K. Donev, M. Kindermann, and P. L. McEuen, Nat. Phys. **2**, 687 (2006).
[8] J. Heo and M. Bockrath, Nano Lett. **5**, 853 (2005).
[9] F. Triozon, S. Roche, A. Rubio, and D. Mayou, Phys. Rev. B **69**, 121410(R) (2004).
[10] See B. Bourlon, C. Miko, L. Forró, D. C. Glattli, and A. Bachtold, Phys. Rev. Lett. **93**, 176806 (2004), and references therein.
[11] H. J. Li, W. G. Lu, J. J. Li, X. D. Bai, and C. Z. Gu, Phys. Rev. Lett. **95**, 086601 (2005).
[12] M. Paillet, P. Poncharal, and A. Zahab, Phys. Rev. Lett. **94**, 186801 (2005).
[13] M. Zdrojek, T. Mélin, H. Diesinger, D. Stiévenard, W. Gebicki, and L. Adamowicz, Phys. Rev. Lett. **96**, 039703 (2006).
[14] M. Zdrojek, T. Mélin, H. Diesinger, D. Stiévenard, W. Gebicki, and L. Adamowicz, J. Appl. Phys. **100**, 114326 (2006).
[15] T. Mélin, H. Diesinger, D. Deresmes, and D. Stiévenard, Phys. Rev. B **69**, 035321 (2004).
[16] This basic description of CNTs is justified by the large tip-CNT distance, making EFM unable to resolve the details of the atomic structure of CNTs, and by the fact that the CNTs are imaged on insulating layers, which makes the EFM measurements sensitive to the CNT charge only but not to the charge location in the CNT shells nor to the CNT dielectric constant.
[17] B. Kozinsky and N. Marzari, Phys. Rev. Lett. **96**, 166801 (2006).
[18] A. Mayer, Phys. Rev. B **75**, 045407 (2007).